A Detailed Physical Explanation of an Aircraft Flutter Mechanism

Luiz Felipi Ribeiro Siqueira [a],
Marcelo Santiago de Sousa [a++*],
Flávio Luiz Cardoso-Ribeiro [b++]
and Sebastião Simões da Cunha Junior [a++]

[a] Federal University of Itajubá – UNIFEI (Av. BPS, 1303, Itajubá, MG), Brasil.
[b] Technological Institute of Aeronautics - ITA, (Praça Marechal do Ar, 50, São José dos Campos, SP), Brasil.

Authors' contributions

This work was carried out in collaboration among all authors. All authors read and approved the final manuscript.

Original Research Article

ABSTRACT

Each dynamic mode (aeroelastic) is made up of torsional and rotational movements. These two movements in each mode were dissociated and the phase, amplitude, damping and frequency of each of these movements were analyzed. The structural resistances of torsion and bending, as well as the bending movement itself, have a damping effect and torsion has a destabilizing effect on the oscillations (if the centre of pressure is ahead of the flexural axis). After a certain speed, bending becomes out of phase with the applied forces. At this point, the bending has an amplifying effect on the oscillations and only the structural stiffness dampens the movement. From the speed at which the bending movement is out of phase with the applied aerodynamic loads, the damping of the mode decreases with speed, until flutter occurs. The type of analysis presented here was only

_____

++ Professor;
*Corresponding author: Email: marcelo.santiago@unifei.edu.br;

possible due to the dissociation of torsion and bending movements in each mode. This is a novelty of this article. And this dissociation was made possible due to the use of the strain-based formulation, also called here as methodology NFNS_s (Non Linear Flight Dynamics – Non Linear Structural Dynamics – strain based formulation). The use of this methodology for this type of analysis was another contribution. The article presents the proposal of a new way of analyzing the aeroelastic stability of aircraft.

Keywords: Aeroelasticity; strain based formulation; flexible airplane; flutter mechanism.

1. INTRODUCTION

The term aeroelasticity designates the field of study interested in evaluating the interactions that are established between the disciplines of aerodynamics, elasticity and dynamics [1]. The multidisciplinary nature of this field can be synthesized by the prediction of the forces acting on the structure by using the aerodynamic theories, the deformations being predicted by the elasticity and the dynamics introducing inertial forces in the system [2]. Inside the field of dynamic aeroelasticity, one of the phenomena that carries most attention is flutter. This phenomenon is considered one of the most relevant in aeroelastic studies and one of the most difficult to predict [3].

The emergence of new technologies, such as the growing use of composite materials in the aeronautical industry, which allows for the construction of aircraft with lower structural weight, and the need for specific missions, which require greater wing span, has allowed for the development of aircraft with greater structural flexibility. In these aircraft with greater structural flexibility, a coupling can be seen between the natural modes of flight dynamics and the structural modes. Modeling and understanding the flight dynamics and aeroelasticity of very flexible aircraft is a current research topic [4,5].

The aeroelasticity of each aircraft is influenced by the aerodynamic, structural and mass distribution properties of the aircraft components. The aerodynamic properties are function of the aircraft's geometry and the structural properties are function of the geometry and materials used. Properties of metallic materials, widely used in the aeronautical industry, are already known. However, the structural properties of composite materials and their effect on structural properties [6,7,8,9], structural modes and aeroelastic response [6,7,8,10] are also a current topic of research. Some research has shown the use of piezoelectric materials to control the aeroelastic response of structures built with composite material [11,12].

Despite the knowledge acquired during the last century, and the recent research aimed at understanding the effect of composite materials on structural modes, on aeroelastic response, on controlling this response, and also on the coupling between aeroelasticity and flight dynamics of very flexible aircraft, the physical mechanism that produces the aeroelastic phenomenon called flutter has not yet been presented in detail in the literature (from the authors' point of view).

According to Bisplinghoff and Ashley [13], the insights that aeroelasticity specialists have are largely mathematical. Although it was pronounced more than forty years ago, it is not common to find a detailed physical explanation that links the mathematical models with the physics of the problem. Generally, the approaches that use eigenvalues to find the instability are focused on plotting frequency and damping ratio charts [1]. None of the actual analysis methods allows a clear, and detailed physical interpretation of what is happening. Although some efforts and insights have already been developed to explain the physics involved in flutter [14,15,13,16], these works do not incorporate the data that can be extracted from eigenvectors, i.e., phase and amplitude. Only the mode shapes are usually plotted in aeroelasticity analyses. Bisplinghoff and Ashley [13] have already mentioned that mode shape and phase variations play a fundamental role in the physical mechanism, since these changes have a great influence on how and where the instability of a system with multiple degrees of freedom begins, but they did not explore in details the use of eigenvectors to explain the flutter mechanism. The new approach presented here considers the data of eigenvalues and eigenvectors to diagnose what is happening on the structure. These analyses show an initial development that was made for an aeroelastic mode, found in a numerical model of a highly flexible aircraft, that exhibited flutter. This is the first step in supporting future analysis aimed to develop a new way of analyzing flutter. The analysis commonly performed in which the different

modes are considered is called here as intermodal analysis. The analysis commonly performed not always considers what happens "inside" the mode. The separation and quantification of bending and torsion deformations allows one deeper and detailed analysis. This type of analysis is called here as intramodal analysis. This is not intended to replace the current forms of analysis that have been developed over the century and which have produced satisfactory results. The intention is simply to present a new way of analyzing the aeroelastic stability of aircraft and to achieve a better physical understanding of the flutter mechanism.

This paper is organized as follows: Section 1 presented the introduction, Section 2 presents the NFNS_s methodology and the equations of motion, Section 3 presents the Aeroflex software, Section 4 presents descriptive data of the analyzed aircraft, Section 5 presents the results and analysis and Section 6 presents the conclusions.

2. NFNS_ METHODOLOGY AND EQUATİONS OF MOTİON

The methodology NFNS_s was developed by Cesnik and his co-workers [17, 18] (Su and Cesnik, 2008). NFNS_s uses a beam formulation to capture nonlinearities of the structural deformations and is also capable to compute large deformations and inertial coupling between elastic and rigid generalized coordinates [18]; (Su, 2008) [19]. Fig. 1 and Equations (1-5) present the equations of motion of a flexible airplane.
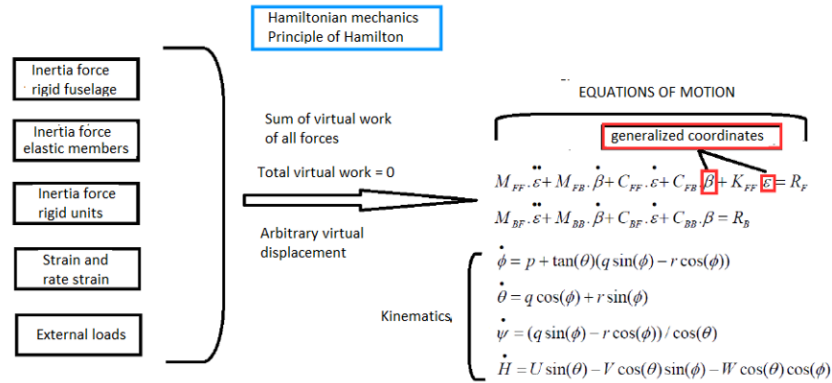

Fig. 1. Equations of motion that describe the dynamics of a flexible aircraft

The complete equations of motion consist of equations (1-5) that contain the dynamics equations together with the rigid body kinematics equations.

$$M_{FF}\,\ddot{\varepsilon} + M_{FB}\,\dot{\beta} + C_{FF}\,\dot{\varepsilon} + C_{FB}\,\beta + K_{FF}\,\varepsilon = R_F$$

$$M_{BF}\,\ddot{\varepsilon} + M_{BB}\,\dot{\beta} + C_{BF}\,\dot{\varepsilon} + C_{BB}\,\beta = R_B$$

$$\dot{\phi} = p + \tan(\theta)(q\sin(\phi) - r\cos(\phi))$$

$$\dot{\theta} = q\cos(\phi) + r\sin(\phi)$$

$$\dot{\psi} = (q\sin(\phi) - r\cos(\phi))/\cos(\theta)$$

$$\dot{H} = U\sin(\theta) - V\cos(\theta)\sin(\phi) + W\cos(\theta)\cos(\phi)$$

$$\dot{p}_N = U\cos(\theta)\cos(\psi) + V(-\cos(\phi)\sin(\psi) + \sin(\phi)\sin(\theta)\cos(\psi)) - W(\sin(\phi)\sin(\psi) + \cos(\phi)\sin(\theta)\cos(\psi))$$

$$\dot{p}_E = U\cos(\theta)\sin(\psi) + V(\cos(\phi)\cos(\psi) + \sin(\phi)\sin(\theta)\sin(\psi)) - W(-\sin(\phi)\cos(\psi) + \cos(\phi)\sin(\theta)\sin(\psi))$$

(1)

Where:

$\beta = [V, U, W, q, p, r]$ is the vector with rigid body degrees of freedom;

ε is the vector with elastic degrees of freedom;

ϕ, θ, ψ are the Euler angles;

H, p_N, p_E are the components of airplane position in relation to the inertial reference frame.

$$M_{FF}(\varepsilon) = J_{h\varepsilon}^T M J_{h\varepsilon}, \qquad M_{FB}(\varepsilon, b) = J_{h\varepsilon}^T M J_{hb}$$
$$M_{BF}(\varepsilon, b) = J_{hb}^T M J_{h\varepsilon}, \quad M_{BB}(b) = J_{hb}^T M J_{hb} + M_{RB} \tag{2}$$

$$C_{FF}(\varepsilon) = C + J_{h\varepsilon}^T M \dot{J}_{h\varepsilon} \qquad C_{FB}(\varepsilon, b) = J_{h\varepsilon}^T M H_{hb} + 2 J_{h\varepsilon}^T M \dot{J}_{hb}$$
$$C_{BF}(\varepsilon, b) = J_{hb}^T M \dot{J}_{h\varepsilon} \qquad C_{BB}(b) = C_{RB} + J_{hb}^T M H_{hb} + 2 J_{hb}^T M \dot{J}_{hb} \tag{3}$$

$$K_{FF} = K \tag{4}$$

$$\begin{bmatrix} R_F \\ R_B \end{bmatrix} = \begin{bmatrix} J_{h\varepsilon}^T \\ J_{hb}^T \end{bmatrix} Ng + \begin{bmatrix} J_{p\varepsilon}^T \\ J_{pb}^T \end{bmatrix} B_F F_{dist} + \begin{bmatrix} J_{\theta\varepsilon}^T \\ J_{\theta b}^T \end{bmatrix} B_M M^{dist} + \begin{bmatrix} J_{p\varepsilon}^T \\ J_{pb}^T \end{bmatrix} F^{pt} + \begin{bmatrix} J_{\theta\varepsilon}^T \\ J_{\theta b}^T \end{bmatrix} M^{pt} + \begin{bmatrix} K_{FF}\varepsilon_0 \\ R_{RB}^{ext} \end{bmatrix} \tag{5}$$

M_{FF}, M_{FB}, M_{BF}, M_{BB} are the components of generalized mass matrix;

C_{FF}, C_{FB}, C_{BF}, C_{BB} are the components of generalized damping matrix;

The matrices Mij e Cij are function of mass distribution and also of the structural deformations;

K_{FF} is the stiffness matrix;

R_F, R_B are the generalized force vectors. These forces are compound by the weight, punctual and distributed forces and moments. Example of punctual force is the thrust and of distributed loads are the aerodynamic forces and moments. These loads are distributed along the structural elements.

Jhε is the derivative of vector h in relation to the structural deformation ε (Sousa, 2013);

Jhb is the derivative of vector h in relation to the vector b;

Jpε, Jθε are components of the matrix Jhe;
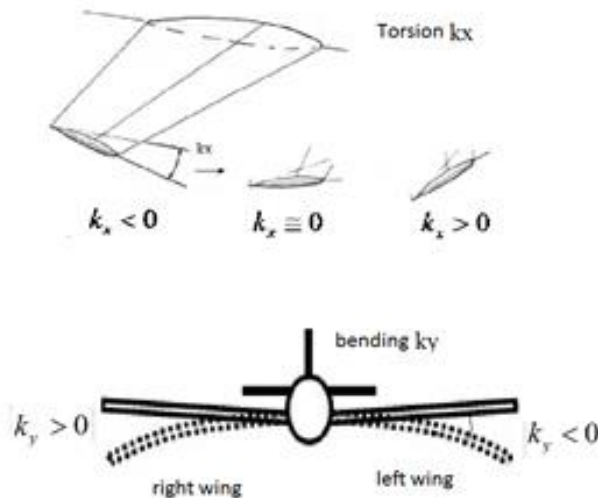
Jpb, Jθb are components of the matrix Jhb.

Fig. 2. Structural deformations (bending ky and twist kx) [20,21] (Sousa, 2013)

Fig. 2 present the type of structural deformations presented in each element: The bending ky and the torsion kx.

Looking at the Eq.(1)-(5), it can be seen that there are equations with degrees of freedom related to the rigid body dynamics and also to the structural dynamics. It means that there is inertial coupling. And there is coupling also in the generalized forces. The derivation of the equations (1) to (5) does not demand only small structural deformations, neither linear structural dynamics. More detailed information about each term in equations (1-5) can be found in Brown, [17], Shearer, [18], Su, (2008), Ribeiro, [19], and Sousa, (2013). Time marching simulations, linearization around a trimmed conditions and calculus of eingenvalues, and eigenvectors can be performed when these equations are used.

3. AEROFLEX SOFTWARE

The Aeroflex software [19] collects information on each structural element, including structural rigidity, mass distribution and inertias, and assembles the structural model described by beams, with their structural and mass properties. The software also collects the aerodynamic information, which includes the aerodynamic forces and moments applied to the quarter chord. The effects of these forces and moments are translated (applied) to the beams that represent the wings and empennages, and in turn, these summed effects are taken to the center of gravity of the aircraft. From the initial conditions, state matrices can be obtained, based on the numerical linearization of the dynamics, around the equilibrium point. From the calculated matrix, the eigenvalues and eigenvectors were obtained, and from these the necessary information for the

aeroelastic stability analysis was obtained. Fig. 3 presents a flowchart of the software AEROFLEX.

The software needed some modifications in order to be ready to capture the eigenvalues and eigenvectors matrices and manage all the data properly. The modifications are better explained on Siqueira, et. al. [22,23] and Siqueira, [22,23]. The modifications were based on changes and developments of new routines to treat the data that AEROFLEX code itself already provides at each trimmed condition. A detailed explanation can be found in Siqueira [22,23]. Fig. 4 presents the functionalities added to the software Aeroflex.

The modifications were made to add functionalities that would make possible to acquire and process the data obtained in each trimmed condition. Originally, the model required a single airspeed, from which the dynamic simulation was done and the results were generated for flight dynamics analysis and applications of flight control techniques. So, the eigenvalues and eigenvectors were already calculated by the code. However, it would be essential to obtain them at a large range of airspeeds in order to plot charts to use as a basis for the physical analysis. In this way, the original code was modified to include an airspeed loop that permits the input of the initial and final airspeeds to simulate the aircraft. The initial and final airspeeds are set before the loop, as well as the speed increment that will be used. At each step of the simulation, the aircraft model is loaded and trimmed to generate the new eigenvalues and eigenvectors matrices, which are stored for future analysis data management. At each airspeed, vectors with eigenvalues and eigenvectors are obtained. At each airspeed step, these vectors are stacked to obtain matrices.
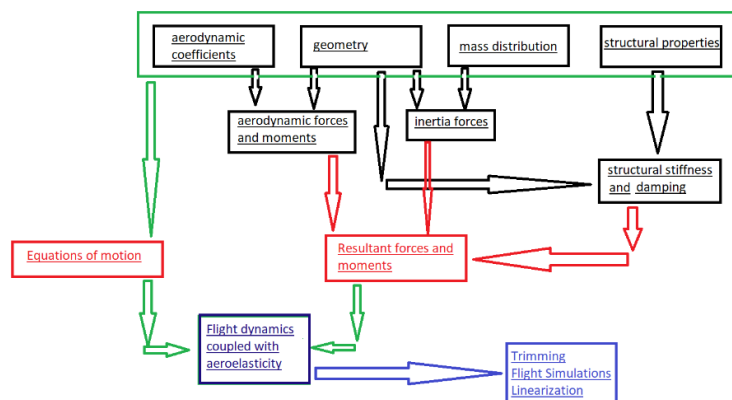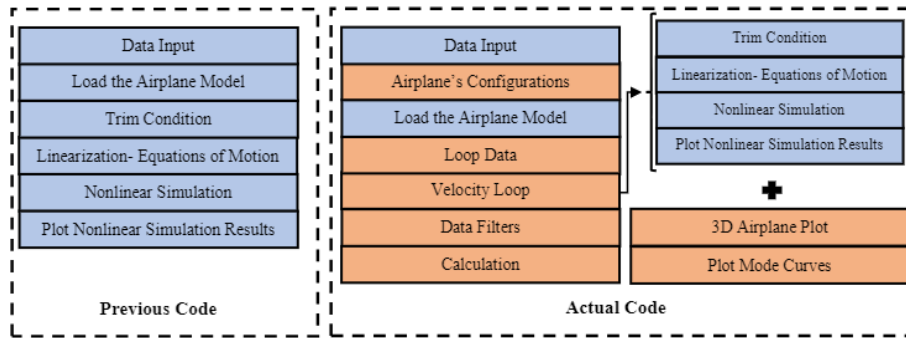

Fig. 3. Aeroflex software flowchart

Fig. 4. Functionalities added to the software Aeroflex

One of the processes developed that has to be emphasized is the data filters. This process involved the selection of aeroelastic modes based on the real and imaginary parts of the eigenvalues. It was necessary to implement a process of mode tracking to order the eigenvalues and the eigenvectors. This was necessary because at each increment of airspeed a new order of eigenvalues/ eigenvectors was generated. In other words, there was randomness in the ordering of eigenvalues and eigenvectors. Although the merge of eigenvalues and eigenvectors was not too large, a method had to be implemented to put the data into the correct sequence that would allow the future treatment to generate the charts. The development of the data filters included four distinct subroutines:

-   Data cleaning: subroutine used to select the aeroelastic modes of interest;

-   Eigenvalues and eigenvectors ordering: responsible for the primary ordering of the data based on the real part of an eigenvalue;

-   Extraction: subroutine used to extract eigenvalues and eigenvectors of conjugate complex pairs;

-   Ordering check: subroutine used to check and reorder eigenvalues and eigenvectors, if necessary.

In short, this code makes a consistency calculation that involves eigenvalues and eigenvectors so that they are in an optimal permutation that guarantees the best sequence between the results.

After the selection of the aeroelastic modes, the code was updated to calculate the values for amplitude, phase, frequency and damping ratio. The first two quantities are extracted from the eigenvectors, while the two latter are from the eigenvalues. The frequency and damping ratio are relative to a specific mode and calculated by Equation 6 and 7, respectively. The phase and amplitude are obtained for each element in each member of the aircraft by Equations 8 and 9, respectively.

$$Frequency = \frac{\sqrt{\left(Re_{va}^2 + Im_{va}^2\right)}}{2\pi} \tag{6}$$

$$Damping\ Ratio = \frac{-100 Re_{va}}{\sqrt{\left(Re_{va}^2 + Im_{va}^2\right)}} \tag{7}$$

$$Phase = \tan^{-1}\left(\frac{Im_{ve}}{Re_{ve}}\right) \tag{8}$$

$$Amplitude = \sqrt{\left(Re_{ve}^2 + Im_{ve}^2\right)} \tag{9}$$

Where:
-   Reva: eigenvalue real part;
-   Imva: eigenvalue imaginary part;
-   Reve: eigenvector real part;
-   Imve: eigenvector imaginary part.

4. AIRPLANE MODEL

The numerical platform AEROFLEX, was adapted in Sousa (2013) for modeling a medium size jet airplane with similar properties to Embraer EMB-190/195 and Boeing 737-200/300. The AEROFLEX uses a methodology that is named here as NFNS_s (Nonlinear Flight Dynamics– Nonlinear Structural Dynamics- strain based formulation).

The aircraft model presented here is the same presented in Sousa et.al., [24], but with two differences: the wing flexural axis is located at 75% mean aerodynamic chord and the structural stiffnesses are six times lower. Fig. 5 presents the aircraft plan view and the aerodynamic plan view, and structural elements of wing and horizontal tail. There are five structural elements on each wing, names as E1, E2, E3, E4, E5. The engines were modeled as rigid units appended on Element 2 (E2).

Fig. 6 presents the flexural axis and mass axis located at 75%mac (mean aerodynamic chord) of each aerodynamic profile and the axis with aerodynamic centers located at 25% mac. The aerodynamic loads are considered to be on the aerodynamic center. There is one offset between the aerodynamic center and the flexural axis.
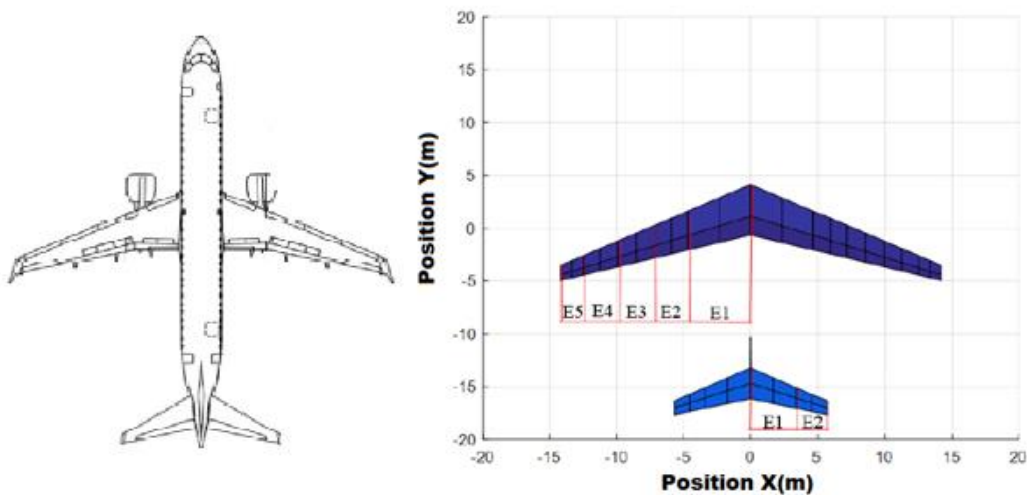

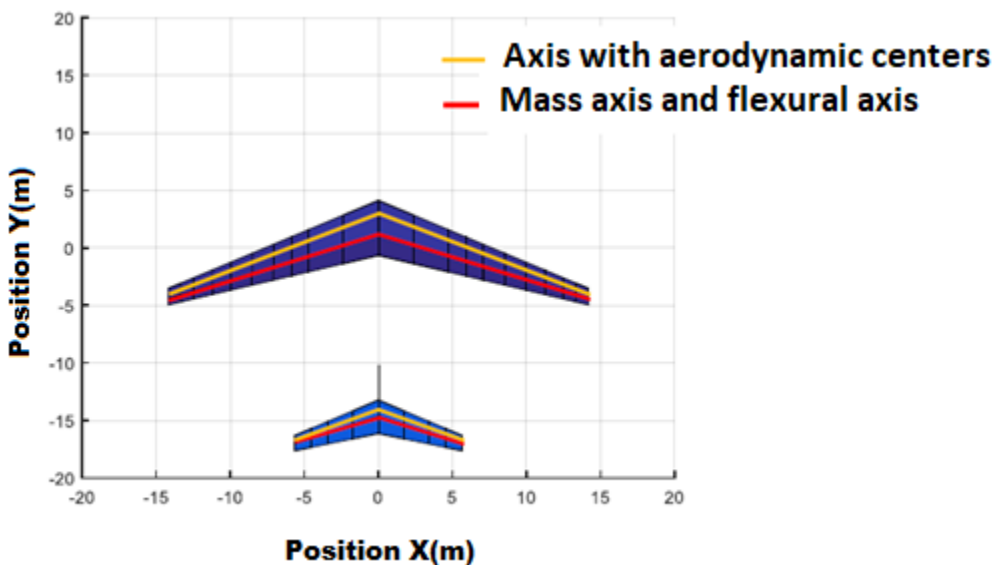**Fig. 5. Aircraft plan view (Doc846, w.d), and Structural elements on the wing [22,23]**

Fig. 6. Flexural axis, mass axis and aerodynamic center axis positions

The aeroelastic model presented is compound by the airplane geometry, aerodynamic, structural and mass distribution data. The airplane was modeled as one assemblage of beams representative of the wing and tails. The fuselage was considered to be rigid and modeled as one rigid mass appended to the airplane. The structural dynamics was modeled with the methodology NFNS_s. The aerodynamics model considers quasi-steady loads. Quasi-steady aerodynamics was considered in order to decrease the computational cost to perform the numerical simulations. The mass was distributed along the wings, tails, engines and fuselage. The next sub-sections present the parameters related to the airplane geometry, aerodynamic, structural and mass distribution data. [25]

Airplane geometry: Airplane geometry values considered more important are presented in Table 1. The Appendix A of this paper contains tables with more detailed information related to the airplane geometry.

The wings and empennages are modeled as flexible beams. The half wing contains five elements and six nodes. Following now are the spanwise wing node coordinates, non-dimensionalised by half span, from root to tip:

$$s_{wing} = \begin{bmatrix} 0.00 & 0.33 & 0.50 & 0.70 & 0.88 & 1.00 \end{bmatrix}$$

The following are the non-dimensional horizontal tail nodes, from root to tip:

$$s_{HT} = \begin{bmatrix} 0.00 & 0.60 & 1.00 \end{bmatrix}$$

and the non-dimensional vertical tail nodes consist only of the root and tip locations:

$$s_{VT} = \begin{bmatrix} 0.00 & 1.00 \end{bmatrix}$$

The idea of choosing 5 elements for the wing, two for the horizontal tail and one for the vertical tail was guaranteeing precise results for analysis of flight dynamics and, at the same time, decrease the number of elements in order to decrease the number of elastic degrees of freedom and, this way, decrease the computational cost. Five elements were implemented for the wing in order to consider the engine position, internal and external aileron positions and to allow the acquisition of similar distribution of aerodynamic loads on the wing. Two elements were implemented to the horizontal tail beams. Only one element was implemented to the vertical tail.

The rigid body representing the engine is connected to the wing node 0.33 (s=0.33) at half-chord.

Table 2 shows the coordinates of beam boundary nodes of wing, horizontal tail and vertical tail. The reference frame origin is located 15.55m behind the aircraft nose. In the present work, the fuselage is rigid and the root nodes of wing, horizontal tail and vertical tail are located in model plane of symmetry. More detailed information about the geometry can be found in Sousa (2013).

The coordinates of Table 2 are in the body reference frame, except for the engine coordinates, which are defined relative to the wing node, where the engine is connected.

Table 1 Aircraft geometry

Parameter	Wing	Horizontal Tail	Vertical Tail
Planform Area	95 m^2	26m^2	20 m^2
Root chord	5.1462 m	3.14 m	4.91 m
Span	28.4 m	11.4 m	5.48 m
Aspect Ratio	8.5	5.0	1.5
Sweep (1/4 chord)	25.0 deg	27.5 deg	40.0 deg
Taper Ratio	0.3	0.56	0.5

Table 2. Coordinates of beam boundary node of wing, horizontal tail and vertical tail [26]

	X (m)	Y(m)	Z(m)
Wing	0.00	1.14	0.00
Horizontal Tail	0.00	-14.68	0.75
Vertical Tail	0.00	-11.55	1.50
Engine	0.00	3.0474	-1.93

Table 3. Fuselage mass, inertia ad CG position

Fuselage Mass (Kg)	24628
CG position (m)	-0.38
I_{xx} (Kg.m^4)	1973300
I_{yy} (Kg.m^4)	6719.2
I_{zz} (Kg.m^4)	1968500

Table 4. Wing mass and inertia distribution

s_{wing}	Mass per unit span (Kg/m)	Inertia I_1 (kg.m)	Inertia I_2 (kg.m)	Inertia I_3 (kg.m)
0.00	1326.00	2252.10	463.30	1788.80
0.33	609.98	702.38	110.44	591.93
0.50	294.22	444.32	69.96	374.36
0.70	81.70	187.43	29.35	158.07
0.88	40.63	78.85	12.34	66.52
1.00	24,0	46.45	7.30	39.15

Table 5. Horizontal tail mass and inertia distribution [26]

s_{HT}	Mass per unit span (Kg/m)	Inertia I_1 (kg.m)	Inertia I_2 (kg.m)	Inertia I_3 (kg.m)
0.00	107.54	204.00	37.00	167.00
0.60	50.96	43.75	7.88	35.63
1.00	24.19	17.66	3.19	14.46

Table 6. Vertical tail mass and inertia distribution

s_{VT}	Mass per unit span (Kg/m)	Inertia I_1 (kg.m)	Inertia I_2 (kg.m)	Inertia I_3 (kg.m)
0.00	186.98	1252.95	369.55	883.40
1.00	48.20	156.17	46.07	110.10
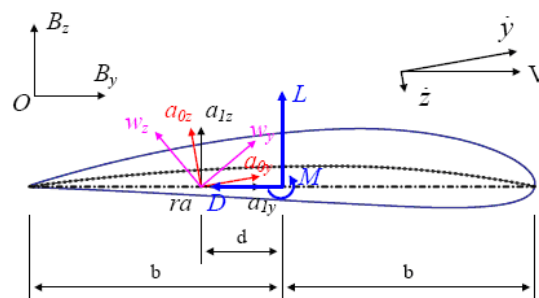
Fig. 7. Airfoil coordinate system and velocity components (Su, 2008)

Mass distribution

Table 3 presents the values of mass, mass moment of inertia and CG position of the fuselage. Tables 4 to 6 present the mass per unit span and cross sectional moments of inertia in each node of the wing and empennages. The total aircraft mass is 45000 kg.

The engine CG position is offset 3.0474 m relative to wing node 0.33 at half chord. The engine mass is 2575 kg (each engine).

Aerodynamic model

The airfoil coordinate system and the aerodynamic equations are presented in Fig. 7 and in equations (10) to (12). In this work, quasi-steady aerodynamic loads were considered. The reason for this choice was the necessity to decrease the computational cost to run the numerical simulations.

$$V \cong \dot{y}, \quad b = c/2, \quad d = ab \tag{10}$$

$$L = C_{L\alpha}\rho b V^2(-\dot{z}/V + (b/2-d)\dot{\alpha}/V) + \rho b \dot{y}^2 C_{L\delta i}\delta i$$

$$M = -0.5\pi\rho b^3 \dot{y}\ddot{\alpha} + 2\rho b^2 \dot{y}^2 (C_{mo} + C_{m\delta i}\delta i) \tag{11}$$

$$D = -\rho b \dot{y}^2 (C_{Do} + C_{D\delta i}\delta i)$$

$$M_x = M + (d + 0,5b)(L\cos(\alpha_t + \alpha_0) - D\sin(\alpha_t + \alpha_0)) \tag{12}$$

where:

$\alpha_t = \arctan(\frac{\dot{z}}{\dot{y}})$, α_0 is the zero lift angle of attack;

b is half the chord length, and ρ is the local air density at altitude H;

$C_{L\alpha} = \dfrac{\partial C_L}{\partial \alpha}$ is the lift curve slope;

$C_{L\delta i} = \dfrac{\partial C_L}{\partial \delta_i}$, $C_{D\delta i} = \dfrac{\partial C_D}{\partial \delta_i}$, $C_{m\delta i} = \dfrac{\partial C_m}{\partial \delta_i}$ are the control derivatives where i=a (aileron), i=e (elevator) , i=r (rudder)

C_{m0} is the zero lift pitching moment coefficient.

The aerodynamic model is complete when the stability derivatives $C_{L\alpha}$, C_{m0}, control derivatives $C_{L\delta i}$, $C_{D\delta i}$, $C_{m\delta i}$ and zero lift angle of attack α_0 are known for each airfoil section on the wing and empennages (Sousa, 2013).

The nomenclature of angle α_0 , and of the stability and control derivatives in the NFNS_s methodology is as commonly used in flight dynamics, but of a different meaning. For example, in flight dynamics discipline, the stability derivative $C_{L\alpha}$ presents the effect of the variation of angle of attack on the aircraft lift, and the control derivative $C_{m\delta e}$ presents the effect of the variation of elevator deflection on the pitching moment around the aircraft CG position. In the NFNS_s methodology, the stability derivative $C_{L\alpha}$ represents the effect of the variation of angle of attack on lift per unit span at the airfoil section considered, and the control derivative

$C_{m\delta e}$ presents the effect of the variation of elevator deflection on the pitching moment per unit span at the airfoil section considered, and around the quarter chord. This different meaning should be understood when developing an aerodynamic model in NFNS_s methodology. More detailed information can be found in Sousa, (2013)

Transonic effects were not considered in this work. Tables 7 to 9 present the parameters needed to model the aerodynamic loads on the wing, horizontal tail and vertical tail, respectively.

Structural model

The structural model is defined by the stiffness matrix K and damping matrix C. These matrices are defined by the values of stiffness and damping at each node. The value of stiffness in each element is the average of stiffness values at the three nodes of the element (Sousa, 2013).

The damping is linearly proportional to stiffness K: $c_i(s) = \alpha_i.k_i(s)$

In all elements of the wing and empennages, the following values were used: α_1=1; α_2=0.02; α_3=0.02; α_4=0.1. Therefore:

✓ the damping c(s) associated with strain ε_x is $1K_1$. Simulations performed have shown that the values of longitudinal deformations ε are small. Although the literature proposes values of damping ratio with the order of 0.02%, the influence of this damping ratio is small, once ε presented small values in the simulations performed;

✓ the damping c(s) associated with the twist strain kx is $0.02K_2$;

✓ the damping c(s) associated with the bending strain ky is $0.02K_3$;

✓ the damping c(s) associated with the bending strain kz is $0.1K_4$;

As mentioned above, only the wing and empennages are modeled as flexible beams, the other components being rigid.

Tables 10 to 12 present the stiffness values at the wing nodes, horizontal tail nodes and vertical tail nodes, respectively:

More details about the model developed can be achieved in Sousa (2013), Sousa et al. (2017).

Table 7. Stability derivatives, control derivatives, and α_0 along the wing span [25]

s_{wing}	$CL\alpha_{wing}$	$C_{L\delta a}$	$C_{D\delta a}$	α_0 (deg)	C_{D0}	C_{m0}	$C_{m\delta a}$
0.00	4.5926	0.0000	0.0000	-2.60	0.0252	0.06	0.0000
0.33	4.7840	0.0000	0.0000	-2.60	0.0252	0.06	0.0000
0.50	4.8797	0.0000	0.0000	-2.60	0.0252	0.06	0.0000
0.70	5.2624	1.7898	0.0387	-2.60	0.0252	0.06	0.1926
0.88	5.5972	4.1496	0.2027	-2.60	0.0252	0.06	0.3974
1.00	5.6929	0.0000	0.0000	-2.60	0.0252	0.06	0.0000

Table 8. Stability derivatives, control derivatives, and α_0 along the HT span

s_{HT}	$CL\alpha_{HT}$	$C_{L\delta e}$	$C_{D\delta e}$	α_0 (deg)	C_{D0}	C_{m0}	$C_{m\delta p}$
0.00	3.937	2.060	0.000	0.000	0.0200	0.000	0.1266
0.60	2.099	1.660	0.000	0.000	0.0200	0.000	0.2266
1.00	0.000	0.000	0.000	0.000	0.0200	0.000	0.0000

Table 9. Stability derivatives, control derivatives, and α_0 along the VT span

s_{VT}	$CL\alpha_{VT}$	$C_{L\delta r}$	$C_{D\delta r}$	α_0 (deg)	C_{D0}	C_{m0}	$C_{m\delta r}$
0.00	3.729	-1.900	0.000	0.000	0.020	0.000	0.167
1.00	3.729	-1.135	0.000	0.000	0.020	0.000	0.358

Table 10. Stiffness distribution along the wing span

s_{wing}	Stiffness K_1 (N.m²)	Stiffness K_2 (N.m²)	Stiffness K_3 (N.m²)	Stiffness K_4 (N.m²)
0.00	$1.8427*10^9$	$1.0406*10^8$	$6.9490*10^7$	$5.7975*10^9$
0.33	$9.6678*10^8$	$3.0603*10^7$	$2.0445*10^7$	$2.1011*10^9$
0.50	$8.9071*10^8$	$2.0220*10^7$	$1.3420*10^7$	$1.3290*10^9$
0.70	$5.5545*10^8$	$7.5660*10^6$	$4.8668*10^6$	$5.6125*10^8$
0.88	$4.1050*10^8$	$3.1627*10^6$	$1.9798*10^6$	$2.3625*10^8$
1.00	$5.2643*10^8$	$2.0547*10^6$	$1.3400*10^6$	$1.3900*10^8$

Table 11. Stiffness distribution along the horizontal tail span

s_{HT}	Stiffness K_1 (N.m²)	Stiffness K_2 (N.m²)	Stiffness K_3 (N.m²)	Stiffness K_4 (N.m²)
0.00	$3.1449*10^9$	$5.4021*10^7$	$3.6977*10^7$	$3.4075*10^9$
0.60	$1.2807*10^9$	$9.1732*10^6$	$6.1740*10^6$	$7.3167*10^8$
1.00	$1.3862*10^9$	$4.0582*10^6$	$2.7577*10^6$	$2.9512*10^8$

Table 12. Stiffness distribution along the vertical tail span [25]

s_{VT}	Stiffness K_1 (N.m²)	Stiffness K_2 (N.m²)	Stiffness K_3 (N.m²)	Stiffness K_4 (N.m²)
0.00	$4.944450*10^9$	$1.734826*10^8$	$1.171463*10^8$	$1.344004*10^{10}$
1.00	$2.470720*10^8$	$2.202781*10^7$	$1.498180*10^7$	$1.675040*10^9$

5. RESULTS

Trimmings were made at different speeds, and the eigenvalues and eigenvectors were calculated for each speed.

With all the results obtained, it was possible to plot some graphs. The frequency and damping ratio are related to the mode, whereas the phase and amplitude are associated with the mode and with each element at each member (wings, horizontal tail or vertical tail). If a member with five elements is chosen, five phase curves will be shown in one graph and five amplitude curves in another graph.

The idea used to explain the physical mechanism was to find a flutter condition and understand what is happening in each part of the aircraft structure. Therefore, simulations with a highly flexible aircraft were performed. The airspeed range analyzed was between 100 and 600 m/s. More than 50 aeroelastic modes were obtained, but just three are presented. So, the three first aeroelastic modes were selected for the physical analysis. Fig. 8 shows the frequency and damping ratio of these three modes analyzed.

It is clear from Fig. 8 that the second mode, M2, is the one that has negative damping ratio and, consequently, flutter. Since this mode is the one which presented flutter, the intramodal analysis was totally focused on it. Figs. 9a and 9b shows a 3D representation of the second mode. Both figures allow the visualization of one positive bending (Up) and negative twist on the left wing and positive bending (down) and positive

twist on the right wing. Structural deformations on the horizontal and vertical tail were not observed.

Fig. 9 illustrates a qualitative format of the aeroelastic mode, demonstrating how a certain part of the aircraft deforms in relation to the equilibrium calculated at the trimmed condition. It is possible to observe the two wings, the horizontal and vertical tail. They do not consider the phase lag present between the elements. The fuselage is not illustrated because the numerical model considers it as a rigid unit. Fig.10 shows the amplitudes and phases for both components, torsion kx and bending ky, for mode 02 and specifically for the right wing, what is analogous to the left one. There are five curves in each chart because each wing is composed of five elements. Element 1 is the first wing element attached to the fuselage. Element 5 is on the wing tip, and Elements 2, 3 and 4 are intermediary (See Fig. 5). The engine is attached to the Element 2 [22,23].

Based on Fig. 10(a), it is noted that the phase values of torsion depart slightly above zero in ascending order and tend to have the same negative phase value (around -10º). When this value is reached, there is a small leap around 225 m/s and a moderate one near to 250 m/s. After these leaps, the values were increased until the flutter velocity, around 425 m/s. The curves of torsion amplitudes have the same behavior among themselves and increase the values until 225 m/s. Reaching the maximum, the torsion amplitudes started to decrease until the flutter airspeed.
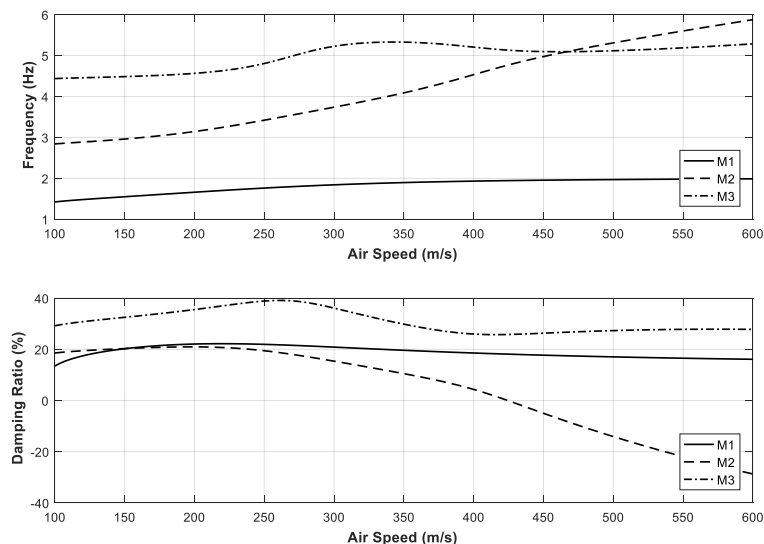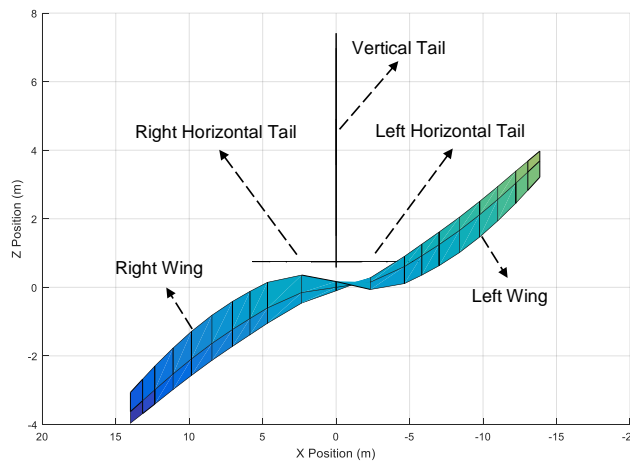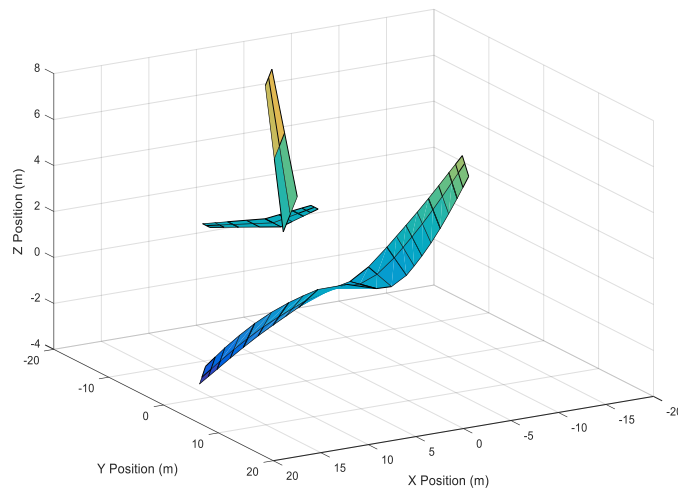

Fig. 8. Frequency and Damping Ratio of the aeroelastic modes

(a)

(b)

Fig. 9. (a) Front view and (b) perspective view of mode 2

The bending phases, shown in Fig. 10(c), began around 0⁰ and had a sudden variation of 180⁰ around 200 m/s, the same velocity in which the minimum amplitude value was achieved. The bending phase values had a considerable changing and presented a smooth variation after the rapid changing. The element 01 did not present this variation, possibly because this element is attached to the fuselage. The element 02 had a different behaviour when compared with the elements 03, 04 and 05, what can be explained by the presence of the engine in this element [24].

The flutter is characterized by the signal change in the damping ratio (positive to negative). This

is equivalent to say that a signal change occurs in the corresponding eigenvalue.

It is evident by intramodal analysis that the torsion and bending presented a phase difference. Phase difference plays a fundamental role in the amount and direction of energy flux between the aerodynamic flow and the structure [16]. This means that the mismatch between bending and torsion creates conditions for a flutter. Before presenting more results, it would be convenient to remember some basic physical concepts, that can be useful. Once the airplane receives one external aerodynamic perturbation, some aerodynamic forces and moments can be produced. Example: gusts produce modifications on the wing lift force (Fig. 11).
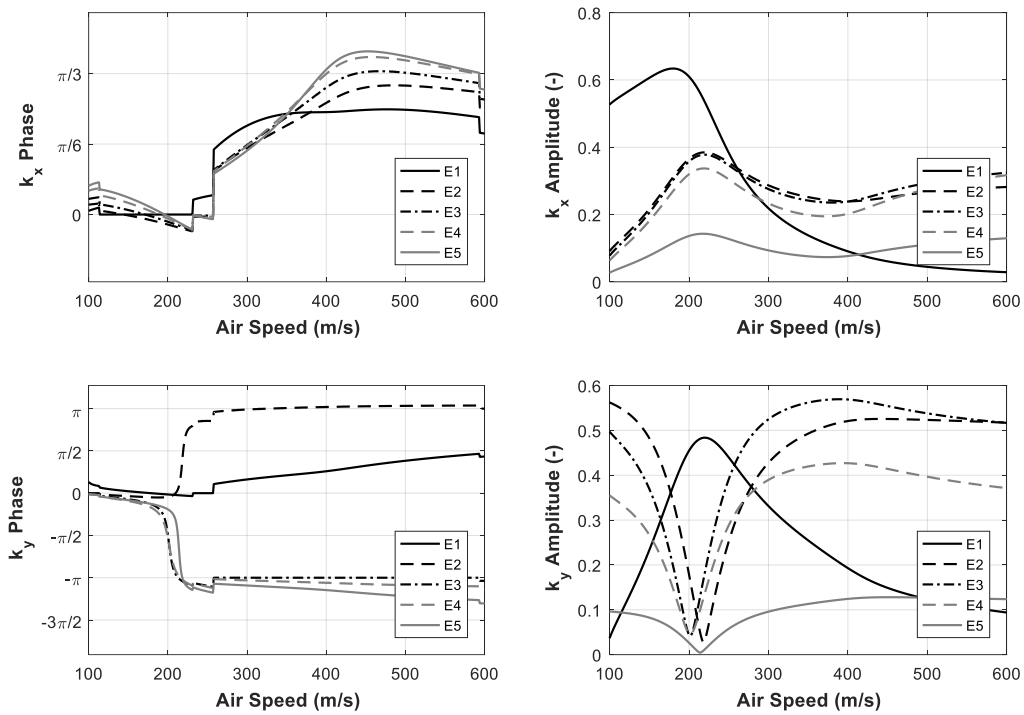
Fig. 10. (a) Phase for torsion kx, (b) amplitude for torsion kx (b), (c) phase for bending ky, (d) amplitude for bending ky
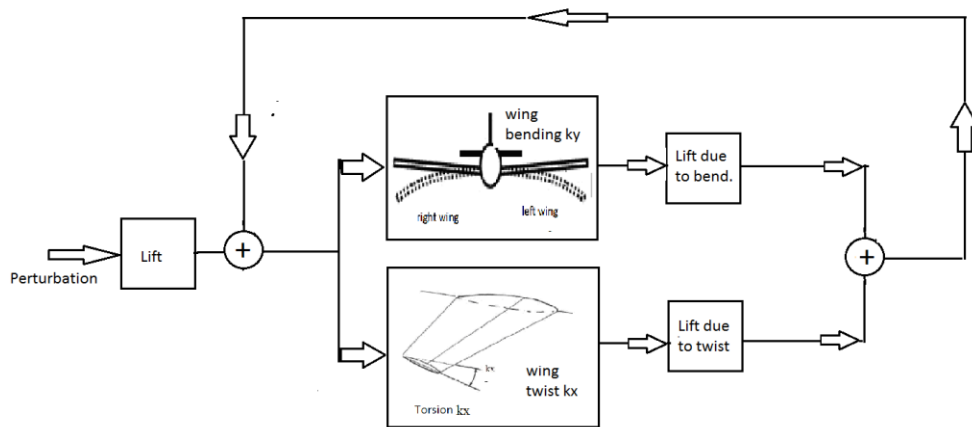

Fig. 11. Mechanism for amplification or damping of structural deformations
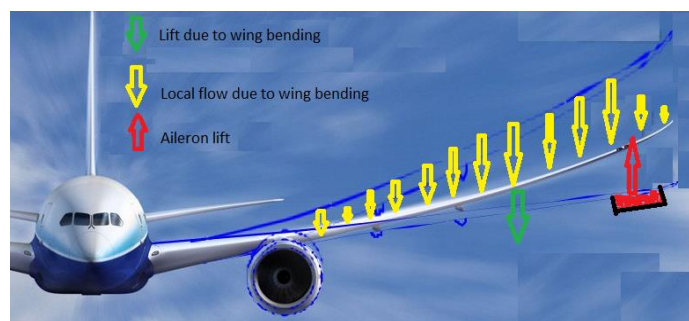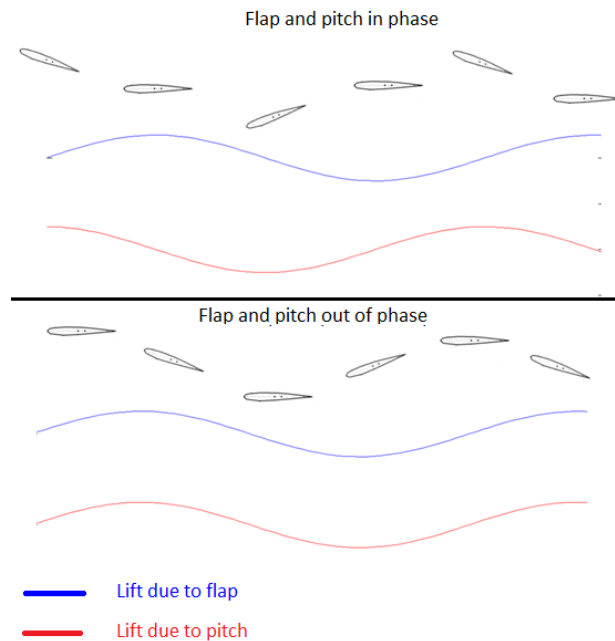

Fig. 12. Damping in external perturbations due to bending deformations (Sousa, 2013), [27].

Fig. 13. Example of phase difference between the pitch (twist) and flap (bending)

This modification on lift force (called here as delta lift force) can produce structural deformations as wing bending and torsion. If the bending deformation has one phase difference smaller that 180 deg, the wing will bend Up, and if the twist has one phase lower than 180 deg, the wing will twist Up (leading edge Up). The consequence is different angles of attack, that will change the lift force. If the wing bending is Up, the local angle of attack will decrease, and the wing lift also (See Fig. 12). So, the bending reaction has one stabilizing effect (it decreases the initial delta lift force, and, as consequence it can dampen the structural oscilations). The bending act as one dynamic damping. It the wing twist Up, the angle of attack will increase, and the wing lift also. So, the wing twist has one destabilizing effect, when the aerodynamic lift force is ahead/ forward than the flexural axis. The angle of attack would increase more, and so, the delta lift force.

Before moving on, it is advisable to better comprehend the concept and meaning of phase difference. Concept: If it is considered one system under periodic perturbation, ex: sinusoidal input, the phase shows the time instant in which the system will respond to the external perturbation. This idea is commonly understood, but its meaning on aeroelastic analysis were not detailed understood during this study. If one plot of structural displacement (xo) versus the derivative of the displacement

(relative to the time, vo, divided by the frequency wn) is made, and if all the possible combinations are plotted, one circle can be obtained (see Fig. 14). If one point of this circle is chosen, the angle obtained is the phase. The phase presents the relation between the structural displacement, and its derivative (Inman, 2014). Its derivative vo is called here as velocity vo. Once these comments and explanations were presented, the analysis done can be presented.

With the results presented for the second mode, it is possible to begin the proposition of the flutter physical mechanism. First, it is essential to point out that the analysis considers five hypotheses:

1ª. The velocity (vo) is responsible for generating the impulse of the movement (bending and/or torsion), i.e., the movement begins with the initial velocity if the element in question is not cantilevered (attached to one fixed point);

2ª. The components of the movement, bending or torsion, with greater velocity module leads the oscillatory movement;

3ª. Only the action of an initial force F is considered and not its variation ΔF generated in the movement over time;

4ª. The proportion of the components (xo and vo) is maintained when the frequency changes;

5ª. The analysis shown is also applied for cases with structural damping.

The aeroelastic mode is composed by torsion and bending deformations, with phase difference. The "in phase" designation is usually made when the angle between the components is 0°. And the "out-of-phase" motion is normally referenced by the literature (Wright and Cooper, 2007) by a 90° difference (or more). When the components are in phase, it means that the bending movement reaches the maximum amplitude almost simultaneously with the torsion motion. In the first quarter of the cycle, the lift produced and the displacement of the structure are positive and then, positive work is done on the airfoil. In the second quarter of the cycle, the lift is positive and the displacement is negative. So, negative work is done on the airfoil. The same occurs for the last two-quarters of the cycle. In short, work close to zero is done [28]. When the phase difference between the motions is 90°, the maximum and minimum of the bending and torsion motions are not reached at the same time. In the two first quarters of the cycles, both displacement and lift are positive. In the last half of the cycle, both magnitudes become negative. So, a work different to zero is done on the airfoil. The motions do not attempt to stabilize, but rather to reinforce themselves [28]. When the movement with a phase difference (between torsion and bending) of 180° is evaluated, the maximum amplitude of the bending movement is counterposed by the minimum torsion and vice-versa. Then, returning and summarizing the data presented previously for the second mode, seen in Figs. 10 and 14:

- **Torsion:** the phase begins close to 10° at 100 m/s, then change the direction and become approximately equal to -10° at 225 m/s. There are this leap and after that, the phase is increased until a maximum value around 60° is achieved at flutter speed, 425 m/s. The amplitude has a maximum value until 225 m/s and decays after this velocity;

- **Bending:** the phases were close to -20° before the phase leap, that occurs with the airspeed around 200 m/s. The phase values had a rapid changing and achieved a value close to ± 200°. After this leap, the phases had smooth behavior. The amplitudes of the elements 02, 03, 04 and 05 have a minimum value after the phase leap, that occurs with the airspeed close to

200 m/s. After this airspeed, the amplitudes started to increase.

The differences seen in the phase occurred practically at the same airspeed in which the amplitudes reach the maximum (torsion) and minimum value (bending). It is possible to subdivide the physical mechanism into two different moments: before and after the phase difference (phase leap). The behavior before and after the phase leap can be arranged like presented in Fig. 14. Each component has a velocity associated vo, which is found by the phase angle.

In Fig.14, the x axis presents the values of vo/wn, where vo is the time derivative of structural displacement and wn is the natural frequency. The y axis presents the structural displacement xo. The angle presents the phase [29]. It is noticed by the Fig. 14 (a) that initially both movements were practically in phase. Despite the similarity, there is a small "advantage" in the speed of torsion motion. That is, this movement leads the behavior of the aeroelastic mode. However, as both components are in phase, the bending stabilizing effect helps to prevent instability. But, the stability mechanism is completely changed when the phase difference occurs, which is demonstrated in Fig. 14(b). The bending inverts the direction of movement (i.e., alters the phase angle in 180°) and the torsion that had a small advantage before and was countered by the stability effects, now has a minor instability effect. The magnitude of the bending speed is practically the same, but acts in the opposite direction, which physically changes the system behavior. When the lift is positive, the bending is negative. This increases the angle of attack, that increases the lift. In addition to this, the torsion component has a reduction in velocity magnitude since the phase is around 60°. The twist deformations keep maintaining one destabilizing effect, but, now the bending has also one strong instability effect. Only the structural bending and twist stiffnesses help to avoid the instability until one defined airspeed value. This stabilizing effect decreases with the airspeed increment. The damping ratio presented on Fig. 8 seems to corroborate with this explanation. While the torsion acts as the mechanism to destabilize the movement, the stiffness of the structure and the aerodynamic effect produced by the bending tend to counteract the instability created. Until the phase difference occurs, the bending and torsion components move together and stability is

ensured by the superiority of the stability effects. After the phase difference (phase leap), the bending starts to act in the direction of instability. The effect of instability increases with the airspeed because the delta aerodynamic force (delta lif force) created is greater than that ocurred before the phase difference. This is maintained until the moment that the structure is unable to counteract the instability, so flutter occurs (See Fig. 15).

Qualitatively, the idea emphasized by this new approach to explain the flutter mechanism is that the component that leads the movement captures more energy input provided by the force and thus leaves a smaller amount to be used by the other component. The bending motion is naturally stable when there is not the phase lag acting upon the system. Therefore, considering only the bending movement, since it is dominant in this case, if it is assumed a force acting upwards, instead of the structure goes upwards too, it goes downwards. So, the effect originated by the bending component tends to destabilize the movement because it causes an opposite movement in relation to the force. And, in addition, there are amplitude variations. After the phase leap, the bending component amplitude starts to grow and the amplitude of the torsion to decrease. Consequently, the effect of instability provoked by bending gains dimension with the airspeed and the damping ratio decreases with the speed until the moment the flutter starts. Assuming a lift force F generated by the action of the flow, if the movement of the components were in phase, the structural movement of torsion and bending would be instantaneous.
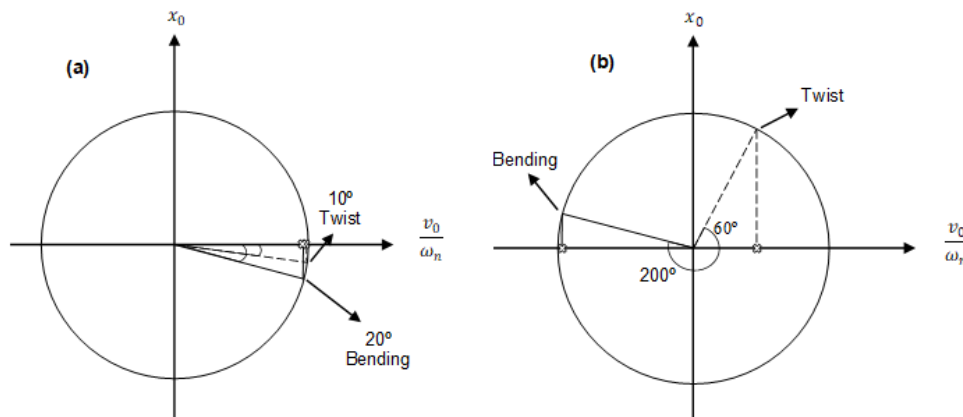

Fig. 14. Scheme for the components (a) before the phase difference and (b) after the phase difference
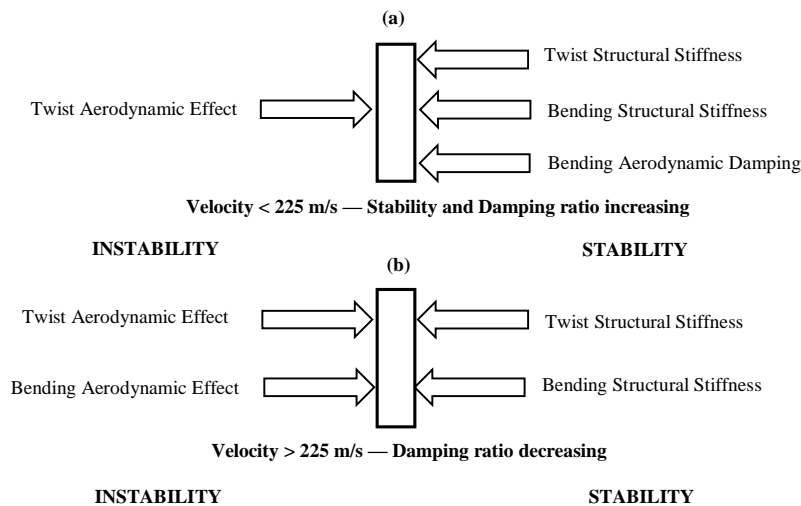

Fig. 15. Instability versus Stability: (a) before the phase difference and (b) after the phase difference

However, with the phase difference, a change in the structural behavior occurs, when there is a temporal lapse between the action of the force and the structure movement. The structure that previously moved upwards now is moving downwards and vice-versa. Although the movement is a combination of bending and torsion, the greater part of instability is directly associated with the bending mechanism. Fig. 8 shows that the structural damping of mode 2 was approximately constant, close to the airspeed of 200 m/s and began to decrease close to 210 m/s. Fig. 10 shows that the torsion phase significantly changed its value close to this speed. These facts seem to be related and the explanation presented seems reliable to the authors. There are important considerations that must be made in relation to the proposition of the physical mechanism. The first one is related to the need to improve/ extend the physical proposition for all the possible cases obtained, which includes other aircraft models. There is the necessity to create a general rule for the physical explanation, possibly incorporating other effects, like the damping ratio. The improvements should be incorporated in future analysis. Although the proposition fits well to mode 2, which presented flutter, element 01 presented a distinction of results when compared to the other elements. This fact cannot be ruled out and prove the urge to evaluate this cantilevered element (element attached to the fuselage). Another research that should be developed is the evaluation of the engine effect on the structure, because the element 02 showed a difference on its phase [30,31].

6. CONCLUSION

In this article a new explanation for the flutter mechanism in aircraft has been proposed. The explanation relies on information on the damping, frequency, amplitudes and relative phases of the torsional and bending movements of each aeroelastic mode, and in each structural element. The use of these parameters has been known and done for a long time. Many aeroelastic stability analyses depend on knowing the structural modes and the frequency and damping curves along the airspeed. The difference here lies in proposing the dissociation of each mode into torsional and bending movements. And in the analysis of each of these movements, as if each were a sub-mode within the structural modes already known. Here we can already use the term intramodal analysis (within modes). This is a novelty in this work. This dissociation was

made possible by the use of the NFNS_s approach. And the use of this approach for this type of analysis was another contribution. The form of analysis proposed was only a first step in the development of a new way of studying and analyzing the aeroelastic stability of aircraft. It is by no means intended to replace the criteria and form of analysis developed throughout the 20th century, but rather to provide a new tool and way of looking at such analysis. The methodology proposed here should be tested on other aircraft, and further research should be carried out to validate the hypotheses presented here. Also, the effect of structural damping should also be considered in future studies. The authors of this paper believe that these are valuable and important research topics for specialists/researchers in aeroelasticity.

ACKNOWLEDGEMENTS

COMPETING INTERESTS

Authors have declared that no competing interests exist.

REFERENCES

1. Wright JR, Cooper JE. Introduction to aircraft aeroelasticity and loads. Chichester, Inglaterra, John Wiley and Sons Ltd. 2007;550.
2. Hodges DH, Pierce GA. Introduction to Structural Dynamics and Aeroelasticity. 2ª Ed., New York, Georgia Institute of Technology, Cambridge University Press. 2011;247.
3. Garrick IE. Reed III WH. Historical development of aircraft flutter. Journal of Aircraft. 1981;18(11):897–912.
DOI: 10.2514/3.57579
4. Cesnik C. Aeroelasticity of very flexible aircraft: Prof. Dewey Hodges. Three-decade Contributions to the Field - AIAA 2023-0585; 2023.
Available:https://doi.org/10.2514/6.2023-0585>. Acessed on April, 15th, 2024
5. Palacios R, Cesnik CES. Dynamics of flexible aircraft: Coupled flight mechanics, aeroelasticity, and conrtrol (Cambridge Aerospace Series, Series Number 52) 1st Edition; 2023.

6. Chandrakar P, Sharma N, Maiti DK. Stochastic buckling response of variable fiber spacing composite plate under thermal environment. Journal of Composite Materials. 2023;57(24).

7. Chandrakar P, Sharma N, Maiti DK. Damage-induced buckling characteristics of thermally loaded variable angle tow laminated plates under uncertain environment. European Journal of Mechanics - A/Solids. 2024;103:105188. Doc846, W.D. E195.
Available:https://doc8643.com/aircraft/E195>. Acessed on April 15th, 2024.

8. Nishad M, Sharma N, Sunny MR, Singh BN, Maiti DK. Stochastic critical buckling speed analysis of rim-driven rotating composite plate using NURBS-based isogeometric approach and HSDT. Mechanics Based Design of Structures and Machines; 2023.

9. Sharma N, Swain PK, Maiti DK, Singh BN. Stochastic frequency analysis of laminated composite plate with curvilinear fiber composite plate with curvilinear fiber. Mechanics of Advanced Materials and Structures. 2022a;29(6).

10. Sharma N, Swain PK, Maiti DK, Singh BN. Static and free vibration analyses and dynamic control of smart variable stiffness laminated composite plate with delamination. Composite Structures. 2022b;280(15).

11. Sharma N, Swain PK, Maiti DK. Active flutter suppression of damaged variable stiffness laminated composite rectangular plate with piezoelectric patches. Mechanics of Advanced Materials and Structures. 2022c;31(6).

12. Sharma N, Swain PK, Maiti DK. Aeroelastic control of delaminated variable angle tow laminated composite plate using piezoelectric patches. Journal of Composite Materials. 2022d;56(29).

13. Bisplinghoff RL, Ashley H. Principles of Aeroelasticity. Dover Publications, New York. 1975;527.

14. Biot MA, Arnold L. Low-speed flutter and its physical interpretation. Journal of Aeronautical Science. 1948;232- 236.

15. Rheinfurth M, Swift F. A new approach to the explanation of the flutter mechanism. Symposium on Structural Dynamics and Aeroelasticity; 1965.
DOI: 10.2514/6.1965-1101

16. Patil M. From fluttering wings to flapping flight- The energy connection. In 42nd AIAA/ASME/ASCE/AHS/ASC Structures, Structural Dynamics, and Materials Conference and Exhibit, Proceedings of AIAA Journal, Seattle, WA. 2001;10.
DOI: 10.2514/6.2001-1460

17. Brown EL. Integrated strain actuation in aircraft with highly flexible composite wings. Dissertation, Massachusetts Institute of Technology (MIT), Cambridge, MA; 2003.

18. Shearer C. Coupled nonlinear and flight dynamics, aeroelasticity and control of very flexible aircraft. Dissertation, University of Michigan, Ann Arbor; 2006.

19. Ribeiro FLC. Dinâmica de vôo de aviões muito flexíveis. Master's Degree Thesis, Technological Institute of Aeronautics, São José dos Campos, Brazil; 2011.

20. AEROSPACEWEB, Wing twist and dihedral; 2000.
Available:https://aerospaceweb.org/question/dynamics/q0055.shtml> . Acessed on April, 9th, 2024.

21. Sofla AYN, Meguid SA, Tan KT, Yeo WK. Shape morphing of aircraft wing: status and challenges. Materials and Design. 2010;31(3):1284-1292.

22. Siqueira LFR. Mode tracking and intramodal aeroelasticity analysis of a highly flexible aircraft with the use of eigenvalues and eigenvectors. Master´s Thesis, Federal University of Itajubá (UNIFEI), Brazil; 2019.

23. Siqueira LFR, Sousa MS, Junior SSC. Flutter analysis tools in a nonlinear structural-flight dynamics numerical platform. 25th ABCM International Congress of Mechanical Engineering (COBEM-2019), Uberlândia, MG, Brazil. 2019;1-8.

24. Sousa MS, Paglione P, Da Silva RGA, Ribeiro FLC, Cunha Júnior SS. Mathematical model of one flexible transport category aircraft. Aircraft Engineering and Aerospace Technology. 2017;89(3):384-396.
DOI: 10.1108/AEAT-12-2013-0230

25. Sharma N, Swain PK, Maiti DK. Uncertainty quantification in free vibration and aeroelastic response of variable angle tow laminated composite plate. Journal of Composite Materials. 2023;57(17).

26. Su W, Cesnik CES. Strain-based geometrically nonlinear beam formulation

for modeling very flexible aircraft. International Journal of Solids and Structures. 2011; 48(16-17): 2349-2360.

27. Quora, What's the airliner with the largest wing flex?; 2016.
Available:https://www.quora.com/Whats-the-airliner-with-the-largest-wing-flex>.
Accessed on April, 12th, 2024

28. Kakkavas C. Computational investigation of subsonic torsional airfoil flutter. Dissertation, Naval Postgraduate School, California; 1998.

29. Inman DJ. Engineering Vibrations. 4ª Ed., Pearson, New Jersey. 2014;8-10.

30. Sharma N, Nishad M, Maiti DK, Sunny MR, Singh BN. Uncertainty quantification in buckling strength of variable stiffness laminated composite plate under thermal loading. Composite Structures. 2021a; 275(1):114486.

31. Sharma N, Swain PK, Maiti DK, Singh BN. Stochastic aeroelastic analysis of laminated composite plate with variable fiber spacing. Journal of Composite Materials. 2021b;55(30).

APPENDIX A

This appendix contains more detailed information related to the airplane geometry.

Table A. 1 Aircraft geometry

Parameter	Descrition	Value
l	Aircraft Length	33.0 m
rf	Fuselage Cross Section Radius	1.5 m
Sw	Wing Planform Area	95 m2
crw	Root chord (in longitudinal axis)	5.1462 m
bw	Wing Span	28.4 m
Aw	Wing Aspect Ratio	8.5
$\Lambda_{c/4w}$	Wing Sweep (1/4 chord)	25.0 deg
$\Lambda_{c/2w}$	Wing Sweep (1/2 chord)	21.23 deg
(x0w,y0w,z0w)	Coordinates of the first node of the wing	(0m; 1.14 m, 0m)
λw	Wing Taper Ratio	0.3
Γ_w	Wing Dihedral	0.0 deg
iw	Wing incidence	3.0 deg
-	Wing profile	NACA 2412
SHT	Horizontal Tail Planform Area	26m2
crHT	Horizontal Tail Root chord	3.14 m
bHT	Horizontal Tail Span	11.4 m
AHT	Horizontal Tail Aspect Ratio	5.0
$\Lambda_{c/4HT}$	Horizontal Tail Sweep (1/4 chord)	27.5 deg
$\Lambda_{c/2HT}$	Horizontal Tail Sweep (1/2 chord)	22.1057 deg
(x0HT,y0HT,z0HT)	Coordinates of the first node of the HT	(0; -14.68 ; 0.75)m
ΛHT	Horizontal Tail Taper Ratio	0.56
Γ_{HT}	Horizontal Tail Dihedral	0.0 deg
IHT	Horizontal Tail incidence	0.0 deg
	Horizontal Tail profile	NACA 0012
SVT	Vertical Tail Planform Area	20 m2
crVT	Vertical Tail Root chord	4.91 m
BVT	Vertical Tail Span	5.48 m
AVT	Vertical Tail Aspect Ratio	1.5
$\Lambda_{c/4VT}$	Vertical Tail Sweep (1/4 chord)	40.0 deg
$\Lambda_{c/2VT}$	Vertical Tail Sweep (1/2 chord)	35.7868 deg
(x0VT,y0VT,z0VT)	Coordinates of the first node of the VT	(0; -11.55 ; 1.5) m
ΛVT	Vertical Tail Taper Ratio	0.5
Γ_{VT}	Horizontal Tail Dihedral	0.0 deg
IVT	Vertical Tail incidence	0.0 deg
-	Vertical Tail profile	NACA 0012
(xENG,yENG,zENG)	Position of Engine	(4.74, 2.40 ,1.93)m

Table A. 2 Geometry of flight control surfaces

Parameter	Description	Value
d_{wt-at}	Distance from the outboard aileron until the wing tip	0.0m
b_a / b_w	Total aileron to wing span ratio	0.3
b_{ai} / b_a	Inboard to total aileron span ratio	0.6
b_{ae} / b_a	Outboard to total aileron span ratio	0.4
d_{HTt-et}	Distance from the outboard elevator until the HT tip	0.0 m
b_e / b_{HT}	Total elevator to HT span ratio	1.0
b_{ei} / b_{HT}	Inboard to total elevator span ratio	0.6
b_{ee} / b_{HT}	Outboard to total elevator span ratio	0.4
d_{VTt-rt}	Distance from the outboard rudder until the VT tip	0.0m
b_r / b_{VT}	Total rudder to VT span ratio	1.0
b_{ri} / b_r	Inboard to total rudder span ratio	0.6
b_{re} / b_r	Outboard to total rudder span ratio	0.4